Semi-analytical solutions for dispersive shock waves in colloidal media

T R Marchant and N F Smyth 2012 J. Phys. B: At. Mol. Opt. Phys. 45 145401

Semi-analytical solutions for dispersive shock waves in colloidal media

T.R. Marchant[1] **and N.F. Smyth**[2]

[1] School of Mathematics and Applied Statistics,
The University of Wollongong,
Wollongong, 2522, N.S.W., Australia.

E-mail: tim_marchant@uow.edu.au

[2] School of Mathematics and Maxwell Institute for Mathematical Sciences,
University of Edinburgh, Edinburgh EH9 3JZ,
Scotland, U.K.

E-mail: N.Smyth@ed.ac.uk

PACS numbers: 42.65.Tg, 42.70.Nq, 42.65.Pc

Submitted to: *J. Phys. B: At. Mol. Phys.*

Abstract.

The diffractive resolution of a discontinuity at the edge of an optical beam in a colloidal suspension of spherical dielectric nanoparticles by a collisionless shock, or dispersive shock wave, is studied. The interaction of the nanoparticles is modelled as a hard-sphere gas with the Carnahan-Starling formula used for the gas compressibility. The governing equation is a focusing nonlinear Schrödinger-type equation with an implicit nonlinearity. It is found that the discontinuity is resolved through the formation of a dispersive shock wave which forms before the eventual onset of modulational instability. A semi-analytical solution is developed in the $(1+1)$ dimensional case by approximating the dispersive shock wave as a train of uniform solitary waves. A semi-analytical solution is also developed for a $(2+1)$ dimensional circular dispersive shock wave for the case in which the radius of the bore is large. Depending on the value of the background packing fraction, three qualitatively different solitary wave amplitude versus jump height diagrams are possible. For large background packing fractions a single stable solution branch occurs. At moderate values an S-shaped response curve results, with multiple solution branches, while for small values the upper solution branch separates from the middle unstable branch. Hence, for low to moderate values of the background packing fraction the dispersive shock bifurcates from the low to the high power branch as the jump height, the height of the input beam's edge discontinuity, is increased. These multiple steady-state response diagrams, also typically found in combustion applications, are unusual in applications involving solitary waves. The predictions of the semi-analytical theory are found to be in excellent agreement with numerical solutions of the governing equations for both line and circular dispersive shock waves. The method used represents a new technique for obtaining semi-analytical results for a dispersive shock wave in a focusing medium.

Keywords. solitary wave, modulation theory, dispersive shock wave, undular bore, colloidal suspension.

1. Introduction

Over the last two decades the mechanical interaction between light and soft matter has received considerable attention, resulting in the emergence of new tools in optics, such as optical tweezers, sensors and selective particle trapping or manipulation, see [1, 2, 3]. One of the attractions of soft media is their large nonlinear response [4, 5, 6], so that nonlinear optical effects can be observed over short, millimetre, distances. An additional attraction is the ease with which their optical properties, including nonlinearity, can be controlled. In the colloidal media considered here, which are composed of a suspension of dielectric nanoparticles, the exceptionally high optical nonlinearity is due to the optical gradient force of an optical beam propagating through the medium changing the concentration or orientation of the colloidal particles. This leads to an intensity-dependent refractive index change and, hence, to a mutual interaction between the colloidal particles and light. Spatial solitary waves can form in a colloidal medium due to the balance between the diffraction of the light beam and this nonlinear particle-light interaction.

In [7, 8, 9] colloidal media governing equations were derived by assuming that the colloidal suspension can be modelled as a hard-sphere gas. They used the Carnahan-Starling formula [10] for the compressibility of the hard-sphere colloid. They then considered (1+1) and (2+1) dimensional colloidal equations and numerically derived exact propagation constant versus power curves for solitary wave solutions. Bistable behaviour was found to occur, with multiple solitary wave solution branches for some parameter values. Numerical investigations of solitary wave interactions for solitary waves of the same power showed that dramatically different interaction behaviour occurred when the interacting solitary waves were from different branches compared with such interaction for solitary waves from the same branch. In the $(2 + 1)$ dimensional case only two solution branches can occur and the bistable behaviour of $(1 + 1)$ dimensional colloidal solitary waves is absent.

The stability of colloidal solitary waves was studied by [11] based on the governing equations of [8]. As no exact solitary waves solutions exist, they used a variational approach to derive semi-analytical solutions for the solitary waves. This approach, termed modulation theory, is based on using a Lagrangian formulation of the governing equations and suitable trial functions. This theory has been used previously to study solitary wave evolution for the nonlinear Schrödinger (NLS) equation [12] and solitary waves in various optical media, such as nematic liquid crystals and colloids, with excellent agreement found with numerical solutions and experimental results [11, 13, 14]. In particular, [11] found excellent comparisons between semi-analytical predictions and numerical solutions for solitary waves in colloids.

For nonlinear dispersive or diffractive wave equations discontinuities are smoothed by dispersion or diffraction resolving the discontinuity into a dispersive shock wave (DSW). Also termed an undular bore or a collisionless shock, a DSW is a modulated wavetrain consisting of solitary waves at its leading edge and linear waves at its trailing edge. The DSW thus gives a smooth transition across the discontinuity. Even though diffraction resolves a discontinuity in bulk media, such as liquid crystals and colloids, the bore in

such bulk media is still commonly referred to as a dispersive shock wave [15, 16, 17, 18]. Mathematically, DSW solutions are derived using Whitham modulation theory [19], with the first such solution derived by Gurevich and Pitaevskii [20] from the modulation equations for the Korteweg-de Vries (KdV) equation, derived by Whitham [19, 21]. Modulation theory develops partial differential equations which describe the evolution of a slowly-varying wavetrain. In general, if these modulation equations are hyperbolic, the wavetrain is modulationally stable and the DSW is found as a simple wave solution, with solitons at its leading edge and linear waves at its trailing edge. If the modulation equations are elliptic, the wavetrain is unstable to long wavelength modulations, termed modulational instability (MI). The modulation equations for focusing NLS-type equations, as in the present work, are elliptic, so that no simple wave, or dispersive shock wave solution, exists. However, the characteristics of the modulation equations for the focusing NLS equation in the linear wave and soliton limits are real [22, 23]. Hence, dispersive shock wave-type solutions can be constructed based on the solitary wave characteristics at the leading edge and the linear wave characteristics at the trailing edge [22, 23]. Of course, this dispersive shock wave-type solution is only the initial behaviour as MI for the waves within it eventually dominates.

The governing equation for wave propagation in colloidal media is a focusing NLS-type equation for which the form of the nonlinearity depends on the assumed nature of the nanoparticle interactions. Hence, the development of a DSW in a colloidal medium is subject to MI and does not persist at long length scales. However, recent experiments show that DSW's can occur in focusing media over experimental length scales. Wan *et al.* [18] showed that a DSW can develop in a focusing photorefractive medium with the MI suppressed by using partially incoherent light. Moreover, the development of a DSW is also observable in nematic liquid crystals. Peccianti *et al.* [24] showed that MI does not occur in such media over typical experimental length scales at low to medium power levels for the optical beam since the nonlocal response of a nematic acts to suppress MI. Hence, it is of interest as to whether experimentally observable DSW's also occur in colloidal media.

Assanto *et al.* [25] considered the formation of a DSW in a nematic liquid crystal, this being an example of a focusing, nonlocal and nonlinear medium. As stated previously, in such a medium the DSW persists for experimentally relevant propagation distances due to nonlocality delaying the onset of MI. Both (1+1) dimensional bores and (2+1) dimensional bores with circular symmetry were considered (termed line and circular bores). A semi-analytical solution was developed for the line undular bore based on approximating it as a train of uniform solitary waves. The predictions of this semi-analytical theory were found to be in excellent agreement with numerical solutions of the governing equations, both for line and circular bores. This semi-analytical solution technique, termed uniform soliton theory, was first developed for a KdV undular bore [26].

In §2, modulation theory is developed for the colloidal media governing equations. A hard-sphere colloidal model is used with the compressibility described by the Carnahan-Starling formula. In §3, the semi-analytical solution for the evolving DSW is developed for the $(1 + 1)$ dimensional line bore geometry. This semi-analytical solution is based on the approximation of the bore as a train of solitary waves. As there is no exact solution

for a steady solitary wave, a variational method is used to obtain an approximation to it. Mass and energy conservation are then used to obtain approximate expressions for the amplitude, spacing and velocity of the solitary waves in the DSW [25, 26]. In §4, the semi-analytical solutions are compared with numerical results for the line and circulars bores, with excellent agreement found. The three different types of solitary wave amplitude, or bore amplitude, versus jump height response diagrams are illustrated. In §5, the results are summarised.

2. Modulation equations

As in previous work [7, 8, 11], let us consider a coherent light beam propagating through a colloidal suspension consisting of uniform hard spheres whose diameter is much smaller than the wavelength of the light forming the beam and whose refractive index is slightly higher than that of the medium in which the colloidal particles are suspended. The governing equations in one spatial dimension in the paraxial approximation are then [7, 8]

$$\begin{aligned} &i\frac{\partial u}{\partial z}+\frac{1}{2}\frac{\partial^2 u}{\partial x^2}+(\eta-\eta_0)\,u=0, \quad |u|^2=g(\eta)-g_0,\\ &\text{with}\ \ g(\eta)=\frac{3-\eta}{(1-\eta)^3}+\ln\eta, \quad g_0=g(\eta_0). \end{aligned} \tag{1}$$

Here u is the slowly varying envelope of the electric field of the light beam and η is the packing fraction of the colloidal particles, with η_0 the background packing fraction. Losses due to Rayleigh scattering have been neglected as these losses are small in the limit of the particle diameter being much smaller than the wavelength of the light [8]. The Carnahan-Starling compressibility approximation has been used to obtain the expression for the state relation g. Alternative models for the compressibility alter the form of g. The Carnahan-Starling approximation is valid up to the solid-fluid transition, which occurs at $\eta=\sqrt{2}\pi/9\approx 0.496$ in a hard-sphere fluid, see [10].

The colloid equations (1) have the Lagrangian

$$\begin{aligned} L=&\,i\,(u^*u_z-uu_z^*)-|u_x|^2+2\,(\eta-\eta_0)\,|u|^2-\frac{4-2\eta}{(1-\eta)^2}\\ &+\frac{4-2\eta_0}{(1-\eta_0)^2}-2\eta\ln\eta+2\eta_0\ln\eta_0+2\,(\eta-\eta_0)\,(1+g_0). \end{aligned} \tag{2}$$

In the present work we are interested in the solitary wave solutions of the colloid equations (1). However, there is no known exact solitary wave solution of these equations. The variational approximation of Marchant and Smyth [11] will then be used for this unknown solitary wave solution as this approximation was found to give solutions in excellent agreement with full numerical solutions of the colloid equations. For a steady-state solitary wave this variational approximation is based on the use of the trial functions

$$u=a\,\mathrm{sech}\,\frac{x-kz}{w}\,e^{i\sigma z+ikx}, \quad \eta=\eta_0+\alpha\,\mathrm{sech}^2\,\frac{x-kz}{\beta} \tag{3}$$

in an averaged Lagrangian formulation of the colloidal equations. The trial function for the electric field is based on the soliton solution of the NLS equation and has amplitude

a and width w. Note that k will be chosen to be the same as the wavenumber of the continuous wave (cw) input profile generating the DSW. It also should be noted that for NLS-type equations the propagation constant k is independent of the solitary wave profile. The packing fraction has amplitude α and width β. As full details are given in [11], only the final (variational) equations for the solitary wave parameters are cited here. These are

$$\begin{aligned}
&1 - 3\alpha w(\Omega_1 - w\frac{\partial \Omega_1}{\partial w}) = 0, \\
&\sigma = -\frac{1}{2w^2} + \frac{\alpha}{w}(2\Omega_1 - w\frac{\partial \Omega_1}{\partial w}) = -\frac{1}{6w^2} + \frac{\alpha \Omega_1}{w}, \\
&4a^2\alpha(\Omega_1 - \beta\frac{\partial \Omega_1}{\partial \beta}) - \beta(\alpha\frac{d\Xi_1}{d\alpha} - \Xi_1) - 4\beta(\alpha\frac{d\Theta_1}{d\alpha} - \Theta_1) = 0, \\
&4\alpha a^2\frac{\partial \Omega_1}{\partial \beta} - \Xi_1 - 4\Theta_1 + 4\alpha\,(1 + g_0) = 0.
\end{aligned} \tag{4}$$

Here

$$\begin{aligned}
&\Omega_1(w, \beta) = \int_0^\infty \operatorname{sech}^2\frac{\zeta}{\beta}\operatorname{sech}^2\frac{\zeta}{w}\,d\zeta, \\
&\Xi_1(\alpha) = 2\int_0^\infty \left[\frac{4 - 2\eta_0 - 2\alpha\operatorname{sech}^2\zeta}{(1 - \eta_0 - \alpha\operatorname{sech}^2\zeta)^2} - \frac{4 - 2\eta_0}{(1 - \eta_0)^2}\right] d\zeta, \\
&\Theta_1(\alpha) = \int_0^\infty \left[\eta_0\ln(1 + \frac{\alpha}{\eta_0}\operatorname{sech}^2\zeta) + \alpha\operatorname{sech}^2\zeta\ln(\eta_0 + \alpha\operatorname{sech}^2\zeta)\right] d\zeta.
\end{aligned} \tag{5}$$

3. Approximate equations for the dispersive shock wave

The simplest initial condition which will lead to the development of a DSW for the focusing NLS-type equation (1) is the jump initial condition

$$u = \begin{cases} a_m e^{ikx}, & x < 0, \\ 0, & x > 0, \end{cases} \qquad \eta = \begin{cases} \eta_m, & x < 0, \\ \eta_0, & x > 0, \end{cases} \tag{6}$$

where a_m is the jump in the electric field amplitude and k is the wavenumber of the continuous wave. As well as the jump in the electric field amplitude u, the first of (6), there is a corresponding jump in the packing fraction, the second of (6). These are linked by the state equation $a_m^2 = g(\eta_m) - g_0$. The initial condition is then a continuous wave in $x < 0$ with nothing in $x > 0$.

To find an approximate solution for the DSW generated by the initial condition (6) we shall use the approximation of [25, 26]. This assumes that the bore consists of a train of solitary wave solutions of (1) of uniform amplitude. This approximation is good for large z as then the bore consists of a large number of individual waves dominated by solitary waves extending from its leading edge [20, 25]. The approximation is not valid near the trailing edge of the bore, where it consists of linear waves. However, this trailing edge region is small in comparison with the leading edge portion for large z.

We then approximate the DSW at z generated by the initial condition (6) by a train of solitary waves. The method determines the amplitude a of the solitary waves generated by the bore, with the other solitary wave parameters determined by (4). The solitary wave amplitude itself is determined using conservation equations [25, 26]. For an initial-boundary

value problem, see [26], all the mass and energy created at the boundary is converted into solitary waves. Hence, the number of solitary waves N and their spacing can be determined. However, for the initial condition (6), which is for an initial value problem on the infinite line $-\infty < x < \infty$, mass and energy can be generated at a different rate to the creation of solitary waves. Hence, the number of solitary wave generated cannot be easily found, but the amplitude of these solitary waves can be.

The colloid equations (1) have the mass conservation equation

$$i\frac{\partial}{\partial z}|u|^2 + \frac{1}{2}\frac{\partial}{\partial x}\left(u^* u_x - u u_x^*\right) = 0. \tag{7}$$

Using Nöther's Theorem on the Lagrangian (2) based on invariances in z gives the energy conservation equation for the colloid equations (1) as

$$\begin{aligned} & i\frac{\partial}{\partial z}\left[|u_x|^2 - 2\left(\eta-\eta_0\right)|u|^2 + \frac{4-2\eta}{\left(1-\eta\right)^2} - \frac{4-2\eta_0}{\left(1-\eta_0\right)^2}\right. \\ & \left. + 2\eta\ln\eta - 2\eta_0\ln\eta_0 - 2\left(\eta-\eta_0\right)\left(1+g_0\right)\right] \\ & + \frac{1}{2}\frac{\partial}{\partial x}\left[u_x^* u_{xx} - u_x u_{xx}^* - 2\left(\eta-\eta_0\right)\left(u^* u_x - u u_x^*\right)\right] = 0. \end{aligned} \tag{8}$$

The conservation laws are integrated from $x = -\infty$ to $x = \infty$ with contributions from the flux terms (x derivative terms) picked up at $x = -\infty$ due to the non-zero boundary condition at $x = -\infty$ from (6). There is no flux contribution from $x = \infty$ due to u being 0 and η being the background value there. Integrating the conservation equations then gives

$$\begin{aligned} & \frac{d}{dz} < M >= k a_m^2, \quad \frac{d}{dz} < H >= k a_m^2 [k^2 - 2(\eta_m - \eta_0)], \quad \text{where} \\ & M = |u|^2, \quad H = \left[|u_x|^2 - 2\left(\eta-\eta_0\right)|u|^2 + \frac{4-2\eta}{\left(1-\eta\right)^2} - \frac{4-2\eta_0}{\left(1-\eta_0\right)^2}\right. \\ & \left. + 2\eta\ln\eta - 2\eta_0\ln\eta_0 - 2\left(\eta-\eta_0\right)\left(1+g_0\right)\right], \quad < . >= \int_{-\infty}^{\infty} . \, dx. \end{aligned} \tag{9}$$

The averaged conservation equations (9) indicate that the rates of mass and energy creation depend on k, the wavenumber of the initial condition. Taking the ratio of the two averaged conservation equations (9) gives

$$< H > - \left[k^2 - 2(\eta_m - \eta_0)\right] < M >= 0 \tag{10}$$

on taking $M = 0$ and $H = 0$ at $z = 0$ as there are no solitary waves initially. The mass-energy ratio (10) also applies to the birth of solitary waves in the DSW and gives a good approximation to the amplitude and width of the solitary waves in the DSW. However, the number N of solitary waves at z depends on the rate of mass and energy creation $< M >_z$ and $< H >_z$ rather than their ratio. These absolute rates are less successful in predicting the number of solitary waves than for boundary value type problems [26]. From the trial functions (3) the mass and energy for a single solitary wave are

$$\begin{aligned} & < M >= 2a^2 w, \quad < H >= P, \quad \text{where} \\ & P = \frac{2}{3}\frac{a^2}{w} + 2k^2 a^2 w - 4\alpha a^2 \Omega_1 + \beta \Xi_1 + 4\beta\Theta_1 - 4\alpha\beta(1+g_0). \end{aligned} \tag{11}$$

Substituting (11) into (10) gives the transcendental equation

$$\frac{2}{3}\frac{a^2}{w} - 4\alpha a^2 \Omega_1 + \beta\Xi_1 + 4\beta\Theta_1 - 4\alpha\beta(1+g_0) + 4a^2 w(\eta_m - \eta_0) = 0, \tag{12}$$

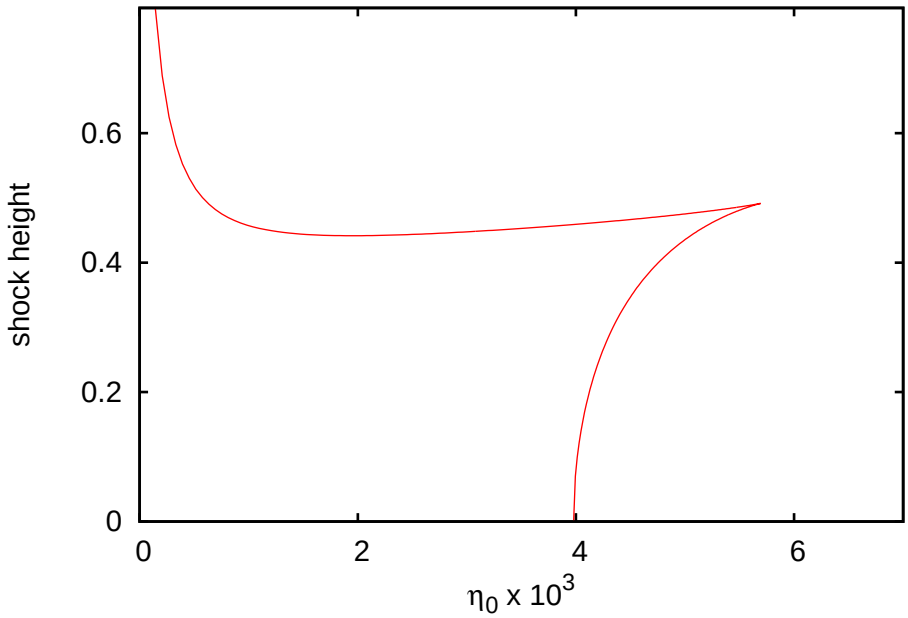

Figure 1. (Color online) The dispersive shock height, a_m, at the bifurcation point versus the background packing fraction η_0.

which determines the amplitude a and width w of the electric field solitary wave and the amplitude α and width β of the packing fraction in terms of the initial jump a_m on using the solitary wave relations (4). The jump in the electric field height a_m is implicitly defined by η_m, the jump in the packing fraction density. Non-zero background wavenumber k causes the bore to move to the right at speed k, but does not affect either the amplitude or number of the waves in the DSW.

Figure 1 shows predictions from the uniform soliton theory. Shown is the dispersive shock height, a_m at the bifurcation points, versus the background packing fraction η_0 as given by (4), (12) and $da_m/da = 0$. If a solitary wave amplitude a versus shock height a_m diagram is considered, then $da_m/da = 0$ is the condition for a bifurcation point to occur in this diagram. The figure shows that for $\eta_0 > 5.69 \times 10^{-3}$ no bifurcation point exists and a single, stable, a versus a_m solution branch occurs. This corresponds to the parameter value separating the bi-stable and mono-stable regimes for the solitary wave solution of the $(1+1)$-D colloid equation, see [8, 11]. For $\eta_0 < 5.69 \times 10^{-3}$ two stable and one unstable branches exists. These three solution branches result in two further types of a versus a_m diagrams. For η_0 in $(3.98 \times 10^{-3}, 5.69 \times 10^{-3})$ an S-shaped a versus a_m response diagram occurs. This kind of S-shaped response curve is a classical one in combustion theory. For example, a reaction-diffusion equation with an Arrhenius reaction term has an S-shaped response curve for which thermal runaway occurs as the solution jumps from the low temperature to the high temperature branch, see [27, 28]. For $\eta_0 > 3.98 \times 10^{-3}$ three solution branches still occur, but in the a versus a_m diagram the upper branch becomes separated from the lower two branches due to part of the curve corresponding to non-physical solutions. Examples are illustrated in Section 4 for the three different types of a

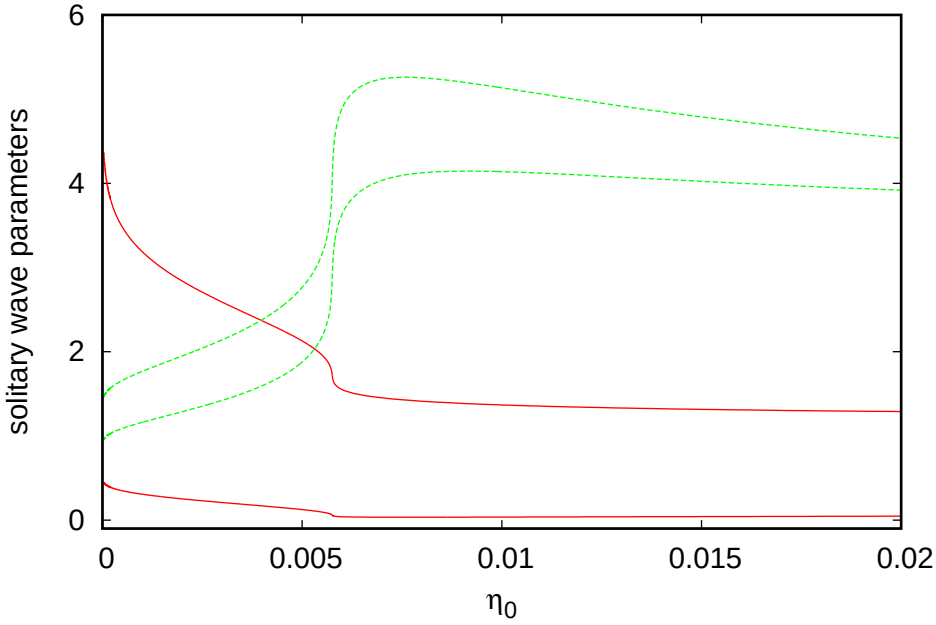

Figure 2. (Color online) Variations of the solitary wave parameters in the DSW versus η_0. Shown are a (upper solid line (red)), α (lower solid line (red)), w (upper dashed line (green)), β (lower dashed line (green)) from uniform solitary wave theory. The other parameter is $a_m = 0.5$.

versus a_m diagrams identified here. In the context of spatial solitary waves this bifurcation behaviour is unusual, with no other known physical systems showing this behaviour.

Figure 2 shows the predictions of the uniform soliton theory. Shown are the amplitudes, a and α, and widths, w and β, of the uniform solitary waves in the DSW, versus η_0, as given by (4) and (12). The initial shock has an amplitude $a_m = 0.5$. For small background packing fractions a DSW consisting of narrow, large amplitude solitary waves is generated by the optical shock, while for large background packing fractions the DSW consists of broader solitary waves of smaller amplitude. The location $\eta_0 \approx 5.69 \times 10^{-3}$ in Figure 2 at which the solitary wave parameters undergo a sharp variation corresponds to the formation of three solution branches in the a versus a_m curve. For small η_0 the solution derived here corresponds to the upper branch of high amplitude. In the limit $\eta_0 \to 0$ the amplitude a of the solitary wave increases indefinitely and the model breaks down. Also, the widths of the electric field and packing fraction solitary waves are comparable, hence the colloidal solitary waves are local, in contrast to the the nonlocal nematic solitary waves, for which $\beta \gg w$, see [25].

4. Results and discussion

In this section numerical solutions of the colloidal equations (1) are compared with the semi-analytical solutions developed for line ((1 + 1)-D) and circular ((2 + 1)-D) DSW's. The numerical solutions were found using a hybrid Runge-Kutta finite-difference scheme.

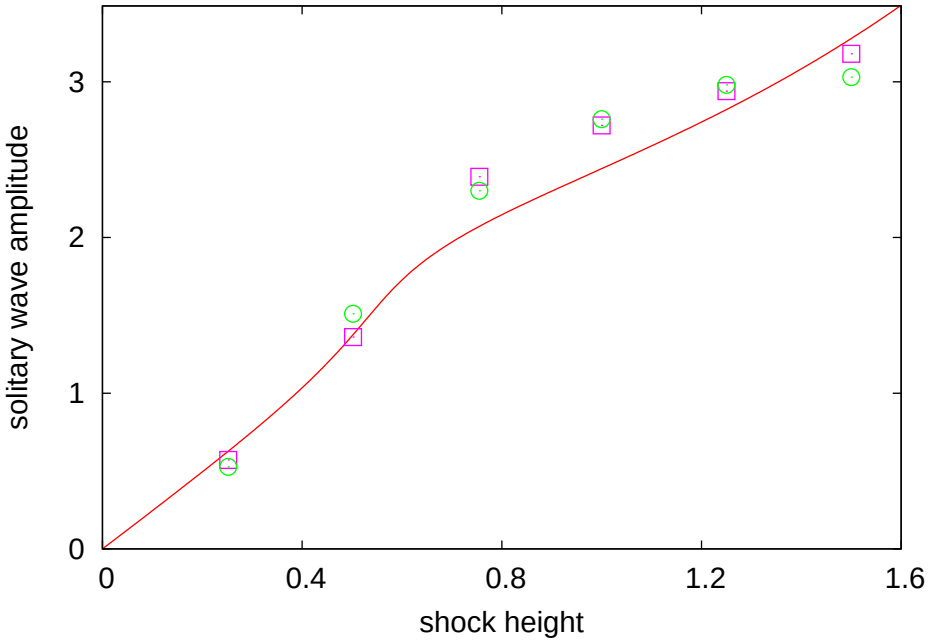

Figure 3. (Color online) Solitary wave amplitude versus shock height, a versus a_m, for the $(1+1)$-D line DSW. Shown are a (solid lines (red)) from uniform solitary wave theory and numerical estimates for the first solitary wave amplitude (squares (pink)) and the average maximum amplitude (circles (green)). The other parameters are $\eta_0 = 1 \times 10^{-2}$ and $k = 0$.

A fourth-order Runge-Kutta scheme was used for the evolution in the propagation direction z (the time-like coordinate) and central finite-differences were used in the spatial domain x. The details of the scheme are given in Appendix A and the step sizes used were $\Delta x = 0.5$ and $\Delta z = 0.05$.

4.1. The line DSW

Figure 3 shows the solitary wave amplitude a versus the shock height a_m for the $(1+1)$-D line DSW. The background packing fraction is $\eta_0 = 1 \times 10^{-2}$ and $k = 0$. Shown are the predictions of uniform solitary wave theory and numerical solutions. Two different numerical estimates of the solitary wave amplitudes are shown. One estimate is the amplitude of the first solitary wave generated by the shock (the initial jump) at the z value for which the solitary wave has fully formed. The second estimate is the maximum solitary wave amplitude in the DSW averaged from the z position at which the first solitary wave has formed until the z value at which MI dominates. An averaging process is needed as there is some oscillation in the solitary wave amplitude as the DSW develops. For this choice of background packing fraction the power versus propagation curve for $(1+1)$-D colloidal solitary waves has a single stable solution branch, see [8, 11]. The behaviour illustrated in Figure 3 is a consequence of this single stable solution branch with the solitary wave amplitude a increasing monotonically as the shock height increases. The comparison between the theoretical predictions and the numerical results is excellent up to $a_m = 1.6$.

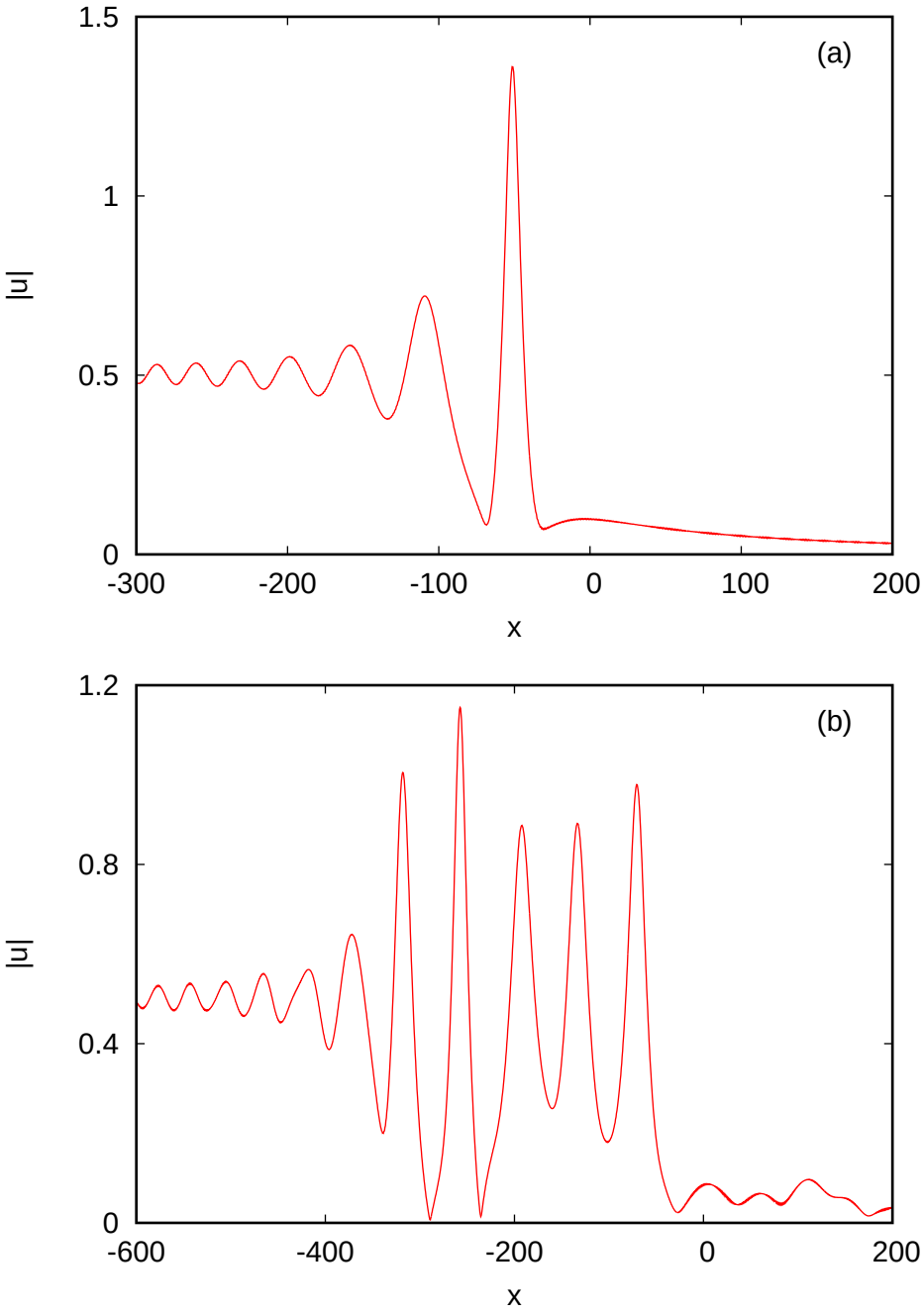

Figure 4. (Color online) The electric field $|u|$ versus x. Shown are the numerical solution at (a) $z = 1150$ and (b) $z = 3000$. The initial packing fraction jump is $\eta_m = 1.26 \times 10^{-2}$ and the background packing fraction is $\eta_0 = 1 \times 10^{-2}$.

The differences range up to 15%, but are typically much lower than this. Results for the packing fraction η are not shown in the Figure, as (numerically) it is an implicit function of $|u|$. For the range $a_m \in [0, 1.6]$ of initial shock heights shown in the Figure the packing fraction amplitude $\alpha \in [0, 0.072]$.

Figure 4(a) shows the numerical solution for $|u|$ versus x at $z = 1150$. The parameter values are the initial and background packing fractions $\eta_m = 1.26 \times 10^{-2}$ and $\eta_0 = 1 \times 10^{-2}$,

respectively. These parameter choices give an initial jump in the electric field of $a_m = 0.502$. The packing fraction η is not shown as its profile is qualitatively the same as that for $|u|$. The propagation distance used corresponds to the location at which the first solitary wave has evolved to its maximum height of $a = 1.36$. The half-width (at an amplitude of 50% of the peak height) of the numerical solitary wave is 12.6. The semi-analytical solitary wave has amplitude $a = 1.39$ and width $w = 4.99$, which gives a half-width of 13.2. The packing fraction amplitude is $\alpha = 4.9 \times 10^{-2}$, the same as the numerical value to 3 d.p. The differences between the semi-analytical predictions and numerical solutions for the solitary wave amplitudes are then very small, less than 5%.

The lead wave in the DSW is stationary. This is in accord with the prediction $k = 0$ of the current uniform solitary wave approximation. A numerical solution for the same parameter values, except with $k = 1$, yields a near identical DSW which is shifted to the right by $x = 1071$. This corresponds to a numerical propagation constant $k = 0.93$, which is very close to the theoretical prediction $k = 1$.

Figure 4(b) shows the numerical solution for $|u|$ versus x at $z = 3000$. At this longer propagation distance five solitary waves have now formed. For a DSW described by a hyperbolic system of modulation equations the DSW is an expansion fan solution of these modulation equations. For the evolution of a step initial condition for the KdV equation the expansion fan, or simple wave solution, was derived by [20] and consists of solitons at the front of the fan, with linear waves at the rear, and has a monotonic decrease in wave amplitude from the front to the back. Here, however, as the modulation equations form an elliptic system and there is no hyperbolic expansion fan, the individual waves do not completely separate [22, 23]. Hence, they continue to interact with each other and they are not ordered by amplitude. At the z value of Figure 4(b) the fourth wave is the largest, with $a = 1.15$. The maximum amplitude in the DSW, averaged over z, is 1.51.

Figure 5 shows the uniform solitary wave amplitude a versus the shock height a_m for the $(1+1)$-D line DSW. The background packing fraction is $\eta_0 = 4 \times 10^{-3}$. Shown are the predictions of uniform solitary wave theory and the numerical solutions. As for Figure 3 two different numerical estimates are shown, the amplitude of the initial solitary wave and also a long z average of the maximum amplitude. For this value of the background packing fraction the solution has an S-shaped response curve with two stable solution branches and one unstable branch. The solution undergoes a bifurcation at $a_m = 0.465$ at which it jumps from the low amplitude branch to the high amplitude branch. At the bifurcation point the amplitude of the solitary waves generated by the initial shock jumps from the low power to the high power stable branch, with a corresponding jump from $(a, \alpha) = (1.45, 4.93 \times 10^{-3})$ to $(a, \alpha) = (2.35, 0.164)$. This behaviour mimics the bi-stable behaviour seen in the power versus propagation constant curve for a solitary wave at low background packing fractions, see [8, 11]. The comparison between the theoretical predictions and the numerical results is very good. The differences between them range up to 20%. On the upper branch there is more variation between the two numerical estimates. As MI occurs for shorter z on the upper branch, the second numerical estimate is averaged over a shorter range of z, leading to a higher variation. In the combustion theory context the upper branch in the region of multiple solutions can be accessed by varying the power or the initial condition.

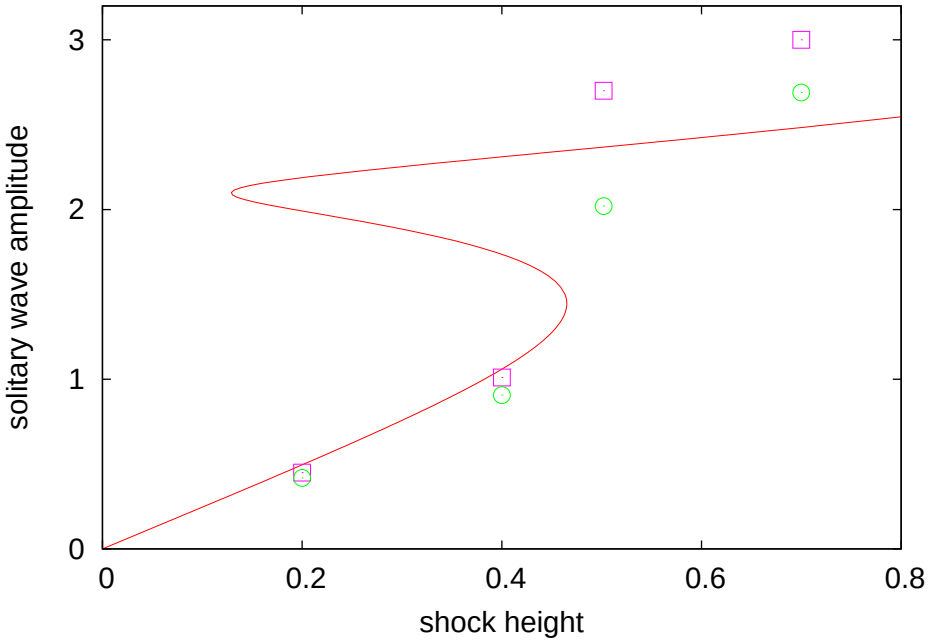

Figure 5. (Color online) Uniform solitary wave amplitude versus shock height, a versus a_m, for the $(1+1)$-D line DSW. Shown are a (solid lines (red)) from uniform solitary wave theory and numerical estimates for the first solitary wave (squares (pink)) and the average maximum amplitudes (circles (green)). The other parameters are $\eta_0 = 4 \times 10^{-3}$ and $k = 0$.

Here, however, it is difficult to access this portion of the upper branch as the initial jump amplitude is the bifurcation parameter. Numerical simulations for $a_m = 0.2$ and 0.4 show that the solution converges to the solution on the lower branch and does not jump to this portion of the upper branch for z values up until MI occurs.

Figure 6 shows the uniform solitary wave amplitude a versus the shock height a_m for the $(1+1)$-D line DSW. The background packing fraction is $\eta_0 = 1 \times 10^{-3}$. Shown are the predictions of uniform solitary wave theory and the numerical solutions. For this value of the background packing fraction the solution again shows three branches, but the upper stable branch is now separated from the unstable branch. This separation occurs because the jump amplitude a_m for the "missing" portion of the S-shaped curve is no longer positive. The solution undergoes a bifurcation at $a_m = 0.43$ at which it jumps from the low amplitude branch to the high amplitude branch. At the bifurcation point the amplitude of the solitary waves generated by the initial shock jumps from $(a, \alpha) = (1.30, 4.14 \times 10^{-3})$ to $(a, \alpha) = (3.18, 0.306)$. The comparisons between the theoretical predictions and the numerical results are again very good. The differences between them range up to 15% on the lower branch and up to 20% on the upper branch.

4.2. The circular DSW

Let us consider the $(2+1)$-D colloid equations (1) with circular symmetry, i.e. $u = u(r, z)$ and $\eta = \eta(r, z)$, where $r = \sqrt{x^2 + y^2}$, with u_{xx} replaced by $\nabla^2 u$. We wish to show that

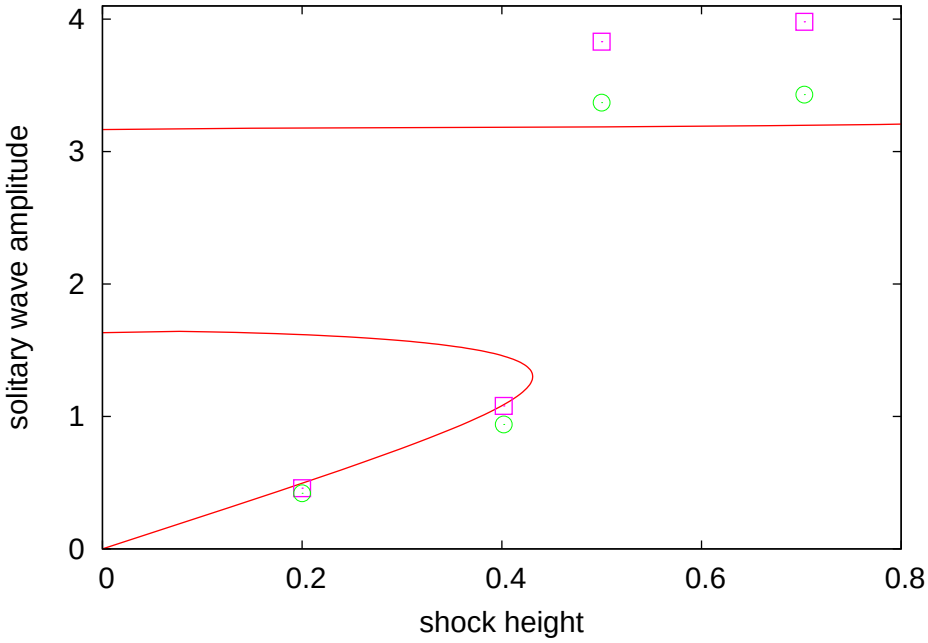

Figure 6. (Color online) Uniform solitary wave amplitude versus shock height (a versus a_m) for the $(1+1)$-D line DSW. Shown are a (solid lines (red)) from uniform solitary wave theory and numerical estimates for the first solitary wave (squares (pink)) and the average maximum amplitudes (circles (green)). The other parameters are $\eta_0 = 1 \times 10^{-3}$ and $k = 0$.

the analytical line bore solution can be used to derive results for the circular bore, so that the boundary condition must approximate the $(1+1)$-D cw at large r. Such a boundary condition is

$$u = \begin{cases} a_m e^{i\theta}, & 0 < r < r_0, \\ 0, & r > r_0, \end{cases} \qquad \eta = \begin{cases} \eta_m, & 0 < r < r_0, \\ \eta_0, & r > r_0 \end{cases} \tag{13}$$

at $z = 0$, where $\theta = (1 - e^{-\alpha_1 r})kr$ and a_m and η_m are linked by the same state relation $a_m^2 = g(\eta_m) - g_0$ as for the $(1+1)$-D case. The form of the phase is chosen so that it has a quadratic chirp near the origin, since $\theta \to \alpha_1 k r^2$ as $r \to 0$. This form ensures that the Laplacian ∇^2 of the boundary condition (13) is bounded in the limit as $r \to 0$. We choose $\alpha_1 = 0.2$, so that the phase is chirp free for $r \geq 50$. Hence, for large r, $\theta \to kr$, which is the $(1+1)$-D cw solution. In contrast to the $(1+1)$-D case, however, the cw is only an exact solution of the $(2+1)$-D governing equations for a stationary bore, for which $k = 0$. For $k > 0$ the cw in (13) is only a valid approximation to the $(2+1)$-D solution for $r \gg 1$. Hence, it will evolve in z, especially near the origin $r = 0$.

Figure 7 shows the numerical solution of the $(2+1)$-D colloid equations (1) for $|u|$ versus r. The other parameters are $\eta_0 = 1 \times 10^{-2}$, $\eta_m = 2.43 \times 10^{-2}$, $r_0 = 600$ and $\alpha_1 = 0.2$. For $k = 0$ the bore is shown at $z = 153$, while for $k = 1$ and $k = 1.5$ the bore is shown at $z = 211$ and 273, respectively. For $k = 0$ a stationary cw exists and the circular bore is qualitatively similar to the corresponding line bore of Figure 4. Note that $|u| \to a_m$ as $r \to 0$ for the stationary circular bore, as the cw is an exact solution of the governing

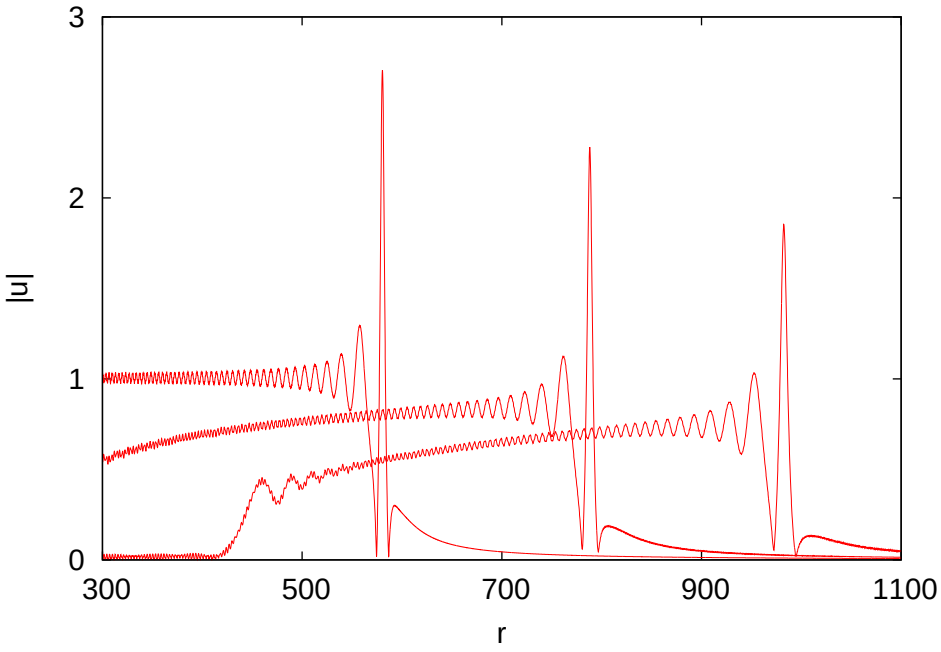

Figure 7. (Color online) Numerical solutions of the (2+1)-D colloid equations (1) versus r. Shown are $|u|$ for $k = 0$ (the left bore) at $z = 153$, $k = 1$ (the middle bore) at $z = 211$ and $k = 1.5$ (the right bore) at $z = 273$. The other parameters are $\eta_0 = 1 \times 10^{-2}$, $\eta_m = 2.43 \times 10^{-2}$, $r_0 = 600$ and $\alpha_1 = 0.2$.

equations. The z value chosen corresponds to the value at which the first solitary wave has fully formed. The peak amplitudes are $a = 2.71$ and $\alpha = 0.274$ at $r = 580$.

For non-zero k the circular bore is quite different to the stationary case as it propagates outwards with a central dark zone forming in which the electric field intensity is low. Qualitatively, this is similar to experimental results for the formation of a circular bore in a defocusing medium [16, 29] (see Figures 2 and 6 of [16] and Figure 5 of [29]). For the non-stationary bores the first solitary wave forms at larger z values. For $k = 1$ the peak amplitude is $(a, \alpha) = (2.28, 0.192)$ at $r = 788$, while for $k = 1.5$ the peak amplitude is $(a, \alpha) = (1.85, 0.110)$ at $r = 982$. These locations correspond to numerical values of $k = 0.99$ and $k = 1.47$, respectively. For the line bore it can be shown analytically that its velocity is k, so that the numerical propagation constants for the circular bores are very close to the theoretical values in $(1 + 1)$-D.

As r increases it can be seen that the amplitudes of the waves in the expanding circular bores decrease. This is due to geometric spreading. A simple geometric optics analysis shows that the electric field amplitude decreases like $a \sim r^{-\frac{1}{2}}$ for large r. Using geometric optics and numerical results for the stationary circular bore gives a prediction for the amplitude of the largest wave in the bore of $a = (580/788)^{\frac{1}{2}} 2.71 = 2.31$ and $\alpha = 0.198$ for the $k = 1$ case. For $k = 1.5$ geometric optics gives predictions of $a = 2.08$ and $\alpha = 0.153$. These results are very close to the actual numerical amplitudes of the expanding bores, with geometric optics explaining about 93% and 73% of the decay in the electric field amplitude in the $k = 1$ and 1.5 cases, respectively.

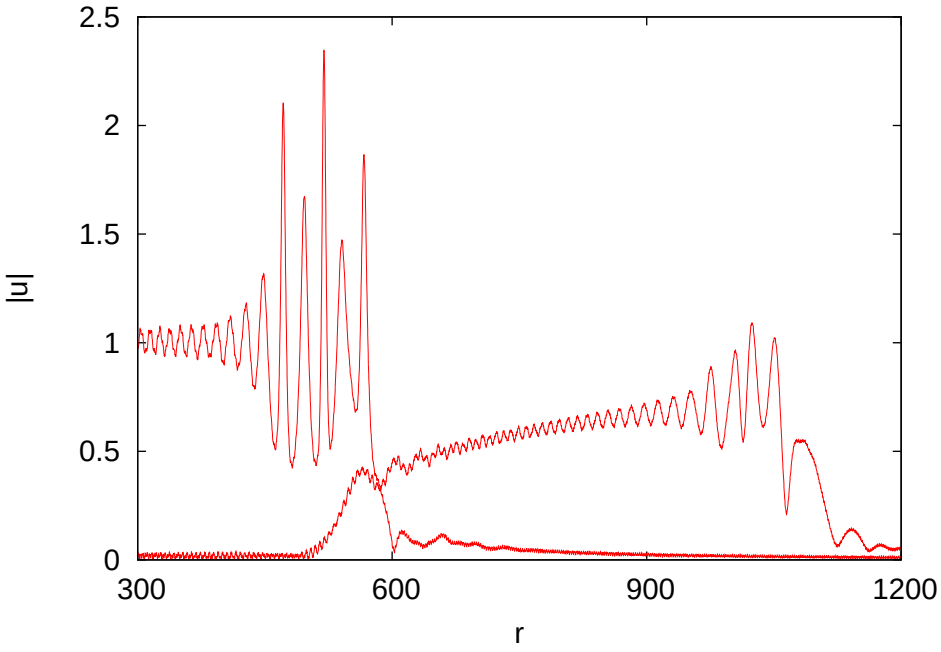

Figure 8. (Color online) Numerical solutions of the (2+1)-D colloid equations (1) versus r. Shown are $|u|$ for $k = 0$ (the left bore) and $k = 1$ (the right bore) at $z = 500$. The other parameters are $\eta_0 = 1 \times 10^{-2}$, $\eta_m = 2.43 \times 10^{-2}$, $r_0 = 600$ and $\alpha_1 = 0.2$

For the line bore as the DSW evolves further the maximum amplitude varies in a complicated manner with z, since the individual waves of the bore are interacting. It was found, however, that the average of the maximum amplitudes over the length of the bore compared well with the predictions from uniform solitary wave theory. For an expanding circular bore, however, the predictions of uniform solitary wave theory must be modified using geometric optics to allow for the effect of geometric spreading. For an expanding circular bore the z-weighted averages of the electric field in a domain extending from $z = 0$ to $z = z_1$ are

$$\frac{a}{z_1}\int_0^{z_1}\frac{dz}{(1+\frac{kz}{r_0})^{\frac{1}{2}}} = \frac{2a}{kz_1}\left[(r_0^2+kr_0z_1)^{\frac{1}{2}} - r_0\right]. \tag{14}$$

The predictions of uniform solitary wave theory for the line bore are $a = 2.48$ and $\eta = 0.231$ for the parameters of Figure 7. For the stationary circular bore, with $r_0 = 600$ and $z_1 = 1200$, the average maximum amplitudes are $a = 2.52$ and $\alpha = 0.239$, a variation of 2% from the line bore theoretical prediction. For an expanding circular bore the predictions of uniform solitary wave theory must be combined with (14). For the $k = 1$ case this gives predictions of $a = 1.69$ and $\alpha = 0.085$ using $z_1 = 1200$, $k = 1$ and the other relevant parameters of Figure 7. The numerical averages for this expanding bore are found to be $a = 1.44$ and $\alpha = 0.054$, which differs by 17% from the theoretical predictions. For the $k = 1.5$ case the theoretical predictions are $a = 1.49$ and $\alpha = 0.059$, while the numerical averages are $a = 1.22$ and $\alpha = 0.035$, a difference of 20%.

Figure 8 shows the numerical solution of the (2+1) dimensional colloid equations (1), $|u|$ versus r, at $z = 500$. The other parameters are $\eta_0 = 1\times10^{-2}$, $\eta_m = 2.43\times10^{-2}$, $r_0 = 600$

and $\alpha_1 = 0.2$. For $k = 0$ the circular bore is stationary and is qualitatively similar to the corresponding line bore of Figure 4(b). As for the line bore case the individual waves do not completely separate, so they continue to interact with each other and are not ordered by amplitude. For the stationary circular bore, $k = 0$, the largest solitary wave has $a = 2.34$ and $\alpha = 0.20$, while the leading edge of the bore is at $r = 600$. For $k = 1$ the bore propagates outwards with the leading edge of the bore at $r = 1074$. The amplitude of the largest wave in this expanding bore is $a = 1.08$, with $\alpha = 0.028$. For this expanding bore $k = 0.95$, very close to the $(1 + 1)$ dimensional estimate of 1.

In summary, it has been found that the analytical theory developed for the line bore geometry also works well for circular bores of large initial radius, giving accurate predictions. Uniform solitary wave theory can be used directly for a stationary circular bore, but must be combined with a geometric optics analysis for an expanding circular bore.

5. Conclusions

The evolution of DSW's in a focusing colloidal medium has been considered both analytically and numerically. The resolution of an initial discontinuity, or optical shock, was examined in both (1+1) dimensions (a line bore) and in (2+1) dimensions with circular symmetry (a circular bore). Semi-analytical solutions which predict the amplitudes of the largest waves in the DSW's were developed using uniform solitary wave theory. This theory assumes that the DSW consists of a train of uniform solitary waves and the amplitudes of these waves are determined from conservation laws for the governing colloid equations. The semi-analytical predictions were found to be in excellent agreement with numerical solutions for both line and circular DSW's.

A non-typical feature of the results is the bifurcation, for small values of the background packing fraction η_0, from a low amplitude to a high amplitude solution branch as the shock height increases. This behaviour is common in combustion theory, but is is very unusual in applications involving solitary waves or optical media.

Due to solutions of focusing NLS equations being subject to MI the boundary value problems considered here are ill-posed. However, it has been found in other focusing media that DSW's do occur on experimentally observable length scales before MI develops [16, 17, 18].

The method used here to develop an approximate solution for a DSW represents a new way of finding analytical solutions in a focusing medium and gives the unusual result of multiple DSW solutions. Hopefully, this theoretical and numerical study will motivate experimental observations of DSW's in colloidal media, which will then allow the validation of the semi-analytical predictions of this work.

Appendix A. The numerical scheme

The numerical solutions of the colloid equations (1) were obtained using centred finite-differences in the spatial coordinate x and a fourth-order Runge-Kutta method for the

time-like propagation direction z. This method was chosen over pure finite-difference methods due to its high accuracy, relative to its computational cost. The solution was then discretized as

$$u_{m,n} = u(z_m = m\Delta z, x_n = n\Delta x), \tag{A.1}$$
$$\eta_{m,n} = \eta(z_m = m\Delta z, x_n = n\Delta x), \quad n = 1, \ldots, N.$$

The colloid equations can be written in the form of an ode by discretizing the terms involving x-derivatives

$$u_{mz} = f(u_{m,n}) = \frac{i}{2\Delta x^2}(u_{m,n+1} + u_{m,n-1} - 2u_{m,n})$$
$$+ \frac{i}{2}(u_{m,n+1} + u_{m,n-1})(\eta_{m,n} - \eta_0), \quad \text{where} \quad |u_{m,n}|^2 = g(\eta_{m,n}) - g_0.$$

The fourth-order Runge-Kutta method then gives the solution at z_{m+1} as

$$u_{m+1,n} = u_{m,n} + \frac{1}{6}(a_{m,n} + 2b_{m,n} + 2c_{m,n} + d_{m,n}), \tag{A.2}$$
$$\text{where} \quad a_{m,n} = \Delta z f(u_{m,n}), \quad b_{m,n} = \Delta z f\left(u_{m,n} + \frac{a_{m,n}}{2}\right),$$
$$c_{m,n} = \Delta z f\left(u_{m,n} + \frac{b_{m,n}}{2}\right), \quad d_{m,n} = \Delta z f(u_{m,n} + c_{m,n}).$$

The packing fraction η is defined as an implicit function of u. To apply the Runge-Kutta method (A.2) an explicit expression is needed for a small change in η corresponding to a small change in u. Expanding the second of (1) in a Taylor series gives

$$\delta\eta = \frac{u\delta u^* + u^*\delta u}{g'(\eta)}, \tag{A.3}$$

which is used to help calculate the expressions for b, c and d at each z-step in the Runge-Kutta method. Once $u_{m+1,n}$ is found, the corresponding value of $\eta_{m+1,n}$ is calculated by Newton iteration using the second of (1). At the boundaries the values of u and η from (6) at $x = \pm\infty$ are applied. The accuracy of the numerical method at each z-step is $O(\Delta z^4, \Delta x^2)$.

References

[1] M. Daoud and C. E. Williams (eds). *Soft matter physics*. Springer, Berlin, 1999.

[2] D. V. Grier. A revolution in optical manipulation. *Nature*, 424:810–816, 2003.

[3] J. M. Ashkin, J. E. Dziedzic, J. E. Bjorkholm, and S. Chu. Observation of a single-beam gradient force optical trap for dielectric particle. *Opt. Lett.*, 11:288–290, 1986.

[4] M. Peccianti, A. Fratalocchi, and G. Assanto. Transverse dynamics of nematicons. *Opt. Expr.*, 12:6524–6529, 2004.

[5] G. Assanto, A. Fratalocchi, and M. Peccianti. Spatial solitons in nematic liquid crystals: from bulk to discrete. *Opt. Expr.*, 15:5248–5259, 2007.

[6] C. Conti, M. Peccianti, and G. Assanto. Route to nonlocality and observation of accessible solitons. *Phys. Rev. Lett.*, 91:073901, 2007.

[7] M. Matuszewski, W. Krolikowski, and Y. S. Kivshar. Spatial solitons and light-induced instabilities in colloidal media. *Opt. Exp.*, 16:1371–1376, 2008.

[8] M. Matuszewski, W. Krolikowski, and Y. S. Kivshar. Soliton interactions and transformations in colloidal media. *Phy. Rev. A*, 79:023814, 2009.

[9] M. Matuszewski, W. Krolikowski, and Y. S. Kivshar. Bistable solitons in colloidal media. *Photon. Lett. Poland*, 1:4–6, 2009.

[10] J. P. Hansen and I. R. McDonald. *Theory of simple liquids*. Academic Press, London, 1976.

[11] T. R. Marchant and N. F. Smyth. Solitary waves and their stability in colloidal media: semi-analytical solutions. *Dyn. Cont. Disc. Imp. Sys.*, to appear.

[12] W. L. Kath and N. F. Smyth. Soliton evolution and radiation loss for the nonlinear Schrödinger equation. *Phys. Rev. E*, 51:1484–1492, 1995.

[13] A. A. Minzoni, N. F. Smyth, and A. L. Worthy. Modulation solutions for nematicon propagation in non-local liquid crystals. *J. Opt. Soc. Amer. B*, 24:1549–1556, 2007.

[14] G. Assanto, A. A. Minzoni, M. Peccianti, and N. F. Smyth. Optical solitary waves escaping a wide trapping potential in nematic liquid crystals: modulation theory. *Phys. Rev. A*, 79:033837, 2009.

[15] C. Barsi, W. Wan, C. Sun, and J. W. Fleischer. Dispersive shock waves with nonlocal nonlinearity. *Opt. Lett.*, 32:2930–2932, 2007.

[16] W. Wan, S. Jia, and J. W. Fleischer. Dispersive superfluid-like shock waves in nonlinear optics. *Nature Phys.*, 3:46–51, 2007.

[17] W. Wan, D. V. Dylov, C. Barsi, and J. W. Fleischer. Dispersive shock waves with negative pressure. *CELO/QLES*, 1-5:2910–2911, 2009.

[18] W. Wan, D. V. Dylov, C. Barsi, and J. W. Fleischer. Diffraction from an edge in a self-focusing medium. *Opt. Lett.*, 35:2819–2821, 2010.

[19] G. B. Whitham. *Linear and Nonlinear Waves*. J. Wiley and Sons, New York, 1974.

[20] A. V. Gurevich and L. P. Pitaevskii. Nonstationary structure of a collisionless shock wave. *Sov. Phys., J. Exp. Theor. Phys.*, 33:291–297, 1974.

[21] G. B. Whitham. Nonlinear dispersive waves. *Proc. Roy. Soc. Lond. A*, 283:238–261, 1965.

[22] G.A. El, A.V. Gurevich, V.V. Khodorovskii and A.L. Krylov. Modulational instability and formation of a nonlinear oscillatory structure in a "focusing" medium. *Phys. Lett. A*, 177:357–361, 1993.

[23] A.M. Kamchatnov, S.A. Darmanyan and F. Lederer. Formation of solitons on the sharp front of the pulse in an optical fiber. *Phys. Lett. A*, 245:259–264, 1998.

[24] M. Peccianti, C. Conti, and G. Assanto. Optical modulational instability in a non-local medium. *Phy. Rev. E*, 68:025602(R), 2003.

[25] G. Assanto, T. R. Marchant, and N. F. Smyth. Collisionless shock resolution in nematic liquid crystals. *Phy. Rev. A*, 78:063808, 2008.

[26] R. H. J. Grimshaw and N. F. Smyth. Resonant flow of a stratified fluid over topography. *J. Fluid Mech.*, 169:429–464, 1986.

[27] T. R. Marchant and B. Liu. The steady-state microwave heating of slabs with small arrhenius absorptivity. *J. Engng. Math.*, 33:219–236, 1998.

[28] B. Liu and T. R. Marchant. The microwave heating of two-dimensional slabs with small arrhenius absorptivity. *IMA J. Appl. Math.*, 62:137–162, 1999.

[29] N. Ghofaniha, C. Conti, G. Ruocco, and S. Trillo. Shocks in nonlocal media. *Phy. Rev. Lett.*, 99:043903, 2007.